JOURNAL OF GEOPHYSICAL RESEARCH, VOL. 112, D10S32, doi:10.1029/2006JD007426, 2007

Prediction of cloud condensation nucleus number concentration using measurements of aerosol size distributions and composition and light scattering enhancement due to humidity

Barbara Ervens,[1,2] Michael Cubison,[3,4] Elisabeth Andrews,[2,3] Graham Feingold,[2] John A. Ogren,[2] Jose L. Jimenez,[3,5] Peter DeCarlo,[3,6] and Athanasios Nenes[7]

Received 21 April 2006; revised 22 November 2006; accepted 4 January 2007; published 14 March 2007.

[1] A cloud condensation nucleus (CCN) closure experiment is carried out using data from the Chebogue Point, Nova Scotia, ground site during the International Consortium for Atmospheric Research on Transport and Transformation (ICARTT) field experiment in 2004. The number concentration of CCN at five supersaturations ($\sim$0.07% to $\sim$0.5%) is predicted from measurements of aerosol size distribution, composition, and hygroscopic growth and is compared to measured CCN concentrations. It is shown that CCN can be predicted quite reliably using measured size distributions, a simple aerosol model to derive the solute-to-water mole ratio, and the diameter growth factor $g(RH)$ or the optical growth factor $f(RH)$. The mean error ranges from an overestimate in CCN of $\leq$5% at high supersaturation to a factor of 2.4 at low supersaturation with regression coefficients r^2 of 0.90 and 0.53, respectively. The poor agreement at low supersaturation is primarily a result of high flow rates in the CCN counter that prevented small particles from growing to detectable sizes. Precise knowledge of the temperature gradient, and flow rates of the instrument, is essential to establish the correct supersaturation, particularly at low supersaturation, where errors translate into a large percentage of the activated number. There may also be some contribution from simplified composition assumptions, e.g., neglecting variability with size and/or mixing state. The mostly oxygenated organic aerosol could be modeled as insoluble, within the above uncertainties, from the point of view of hygroscopicity and activation. The generality of these conclusions will have to be tested at other locations.

Citation: Ervens, B., M. Cubison, E. Andrews, G. Feingold, J. A. Ogren, J. L. Jimenez, P. DeCarlo, and A. Nenes (2007), Prediction of cloud condensation nucleus number concentration using measurements of aerosol size distributions and composition and light scattering enhancement due to humidity, *J. Geophys. Res.*, *112*, D10S32, doi:10.1029/2006JD007426.

1. Introduction

[2] The subset of atmospheric aerosol particles known as cloud condensation nuclei (CCN) are particularly important in climate studies because they are hygroscopic and represent the particles on which cloud droplets form. Their ability to scatter and absorb radiation is influenced by ambient humidity and has important implications for radiative forcing of climate and cloud formation. The ability of an aerosol particle to act as a CCN depends on the extent to which it takes up water vapor, which in turn depends on many factors such as size and composition.

[3] In recent years, the advent of new, commercially available instruments that measure CCN at specified supersaturation values (S) has made it more practical to extend earlier studies and examine more closely the relationship between particle size distribution, composition, hygroscopic properties, and particles' ability to act as CCN. The simultaneous measurement of all of these properties followed by their cross comparison using an activation model, often called "CCN closure," is a self-consistency check on our understanding of the system. Several studies have attempted to address the connection between aerosol growth at subsaturated conditions and their effectiveness as CCN [e.g., *Liu et al.*, 1996; *Covert et al.*, 1998; *Snider and Brenguier*, 2000; *Dusek et al.*, 2003; *Broekhuizen et al.*, 2006]. On the basis of these studies, parameterizations have been developed for the description of the relationship between growth factors and CCN activation [e.g., *Brechtel and Kreidenweis*,

[1]Atmospheric Science Department, Colorado State University, Fort Collins, Colorado, USA.
[2]Earth System Research Laboratory, NOAA, Boulder, Colorado, USA.
[3]Cooperative Institute for Research in Environmental Sciences, University of Colorado, Boulder, Colorado, USA.
[4]School of Earth, Atmospheric and Environmental Sciences, University of Manchester, Manchester, UK.
[5]Department of Chemistry and Biochemistry, University of Colorado, Boulder, Colorado, USA.
[6]Department of Atmospheric and Oceanic Sciences, University of Colorado, Boulder, Colorado, USA.
[7]Schools of Earth and Atmospheric Sciences and Chemical and Biomolecular Engineering, Georgia Institute of Technology, Atlanta, Georgia, USA.

0148-0227/07/2006JD007426$09.00

2000]. These parameterizations require input data such as the growth factor at a given relative humidity (RH), and information on particle composition.

[4] One of the means of determining hygroscopic growth is through measurement of the diameter growth factor $g(RH)$, defined as the ratio of the diameter of a particle at a high RH (e.g., 90%) to its dry diameter (typically 10% RH). In many studies, $g(RH)$ has been determined using Hygroscopic Tandem Differential Mobility Analyzer (HTDMA) measurements [*Rader and McMurry*, 1986]. The instrument preselects a size of aerosol using the first Differential Mobility Analyzer (DMA), conditions the monodisperse population at a given, higher, RH and then passes the particles through a second DMA that is also operated at the higher RH. Growth factors are thus expressed for given sizes, as selected by the first DMA, or size ranges.

[5] In this paper we will address the utility in CCN prediction of an alternative measure of particle growth, namely the enhancement in light scattering due to uptake of water vapor. The aforementioned growth factor is typically referred to as $f(RH)$ [*Covert et al.*, 1972; *McInnes et al.*, 1998] and is measured in a manner analogous to $g(RH)$. The aerosol light scattering is first measured in a nephelometer at a reference (dry) RH (typically less than 40%). Upon exiting the reference nephelometer the air is exposed to a humidifier where it is conditioned to an elevated RH. The resulting ''humidified light scattering'' is then measured in a second nephelometer. Unlike $g(RH)$, $f(RH)$ is expressed as a mean growth factor for the entire (polydisperse) population of particles. Growth factors are often quoted in terms of either two- or three-parameter fits to the data [*Kasten*, 1969; *Kotchenruther et al.*, 1999], from which values at intermediate RH can be calculated. For nephelometers that measure the scattering coefficient at a number of wavelengths, e.g., 450 nm, 550 nm, and 700 nm, $f(RH)$ can be reported at each wavelength. The dependence of scattering on the ratio of particle size to wavelength means that scattering at each wavelength is weighted by a different part of the size distribution [e.g., *Twomey*, 1977]. The blue wavelength (λ = 450 nm) is more sensitive to the sizes that are important for CCN closure. However, the size range of activated particles usually also includes smaller sizes that are not efficient light scatterers, even at 450 nm.

[6] During the summer of 2004, the International Consortium for Atmospheric Research on Transport and Transformation (ICARTT) field experiment took place in the north eastern USA and Canada. The primary goal of the experiment was to study the transport and transformation of pollution of North American origin as it moved eastward over the Atlantic Ocean and toward Europe. An instrumented ship, and a number of instrumented aircraft and surface stations measured a variety of gas and particulate atmospheric constituents. This study will focus on data from the ground station at Chebogue Point, Nova Scotia, where the essential components of a CCN closure experiment were available.

[7] We use in situ size distribution measurements together with both $f(RH)$ (at three different wavelengths: λ_1 = 450 nm (blue); λ_2 = 550 nm (green); λ_3 = 700 nm (red)) and $g(RH)$ measurements at a range of particle sizes in order to constrain the aerosol composition and then predict CCN number concentrations at a range of supersaturations. We explore several assumptions about the complexity of aerosol composition and provide insight into how important each of these parameters is for reliable prediction of CCN for this particular data set. We also explore a number of instrumental issues that might be considered in future studies of this kind.

2. Instrumentation

[8] The Chebogue Point ground site (43.74°N, 62.12°W) operated from 1 July to 15 August 2004 during ICARTT and hosted a number of different teams measuring aerosol and gas phase constituents. For the purposes of our study the primary instrumentation used is listed below.

2.1. CCN Counter (DMT, Boulder, Colorado)

[9] This single channel CCN counter [*Roberts and Nenes*, 2005] was programmed to step through a set of five supersaturations (S_1–S_5) and a spectrum of the number of activated CCN (N_{CCN}) as a function of S was recorded every 30 min. The nominal S set points were 0.09%, 0.23%, 0.32%, 0.43% and 0.55%. However, the actual supersaturations can be slightly different for a specific counter, because of small variations in instrument design and temperature measurement. A heat transfer and fluid dynamics model of the CCN instrument [*Nenes et al.*, 2001; *Lance et al.*, 2006] was used to predict the actual S on the basis of recorded temperatures inside the instrument. Calibrations are used to characterize the heat transfer across the wetted walls of the instrument and then supersaturation is calculated on the basis of the recorded temperature gradient, pressure and inlet temperature. The detailed fluid dynamical model of the instrument [*Roberts and Nenes*, 2005] is also used to calculate the (small) supersaturation variations arising from temporal fluctuations in the instrument temperature profile. Two different calculations of S are used here: Predicted CCN are compared at the S_i calculated from the model of the instrument; in a sensitivity test we also used the nominal values of the instrument.

2.2. Differential Mobility Particle Sizer (DMPS, University of Manchester)

[10] The DMPS [*Williams et al.*, 2000] measured the size distribution over the particle diameter range 3 nm < D_p < 810 nm, at a constant RH in the range 35 to 40%, with a temporal resolution of 10 min. The instrument uses two parallel DMAs coupled to Condensational Nucleus (CN) Counters (TSI Models 3025a and 3010) to classify and count particles according to their electrical mobility diameter. The nano- and long-column DMAs measured from 3 to 34 nm and 29 to 817 nm, respectively. The size distribution is measured using both DMAs simultaneously; the overlap region forms the start of the measurement cycle in both DMAs, which thus acquire particle concentration data for the 29 to 34 nm range at the same point in time.

2.3. CN Counter (TSI Model 3010)

[11] The CN counter measured the total particle concentration N. This counter has an efficiency of 50% at D_p = 10 nm and a lower detection limit of 6 nm [*Hämeri et al.*, 2002].

2.4. Humidograph System (NOAA/ESRL/GMD)

[12] The humidograph system for measuring $f(RH)$ consisted of two integrating nephelometers (TSI 3563) which

measure total and back scattering at 3 wavelengths (450, 550, and 700 nm). The RH in the reference nephelometer was maintained at 30–40%, while the humidity conditioning system generated RH usually between 40–95% for measurement in the second nephelometer. (The upper limit of RH was below RH = 90% for ~25% of the time.) From the combination of the "dry" nephelometer and "wet" nephelometer measurements an $f(RH)$ value for the specific 85%/40% values was obtained on the basis of curve fitting. The uncertainty in hourly averaged nephelometer measurements has been calculated to be 8% [*Clarke et al.*, 2002]. Because $f(RH)$, to first order, can be considered the ratio of two independent nephelometer measurements, a rough estimate of $f(RH)$ would be approximately 16%. However, the true uncertainty in $f(RH)$ will be higher because there are also uncertainties in the associated relative humidity measurements and in the fit to the measurement data.

[13] The inlet to the humidograph system (and CCN counter) was equipped with an impactor to exclude particles and cloud droplets larger than 5 μm diameter, and every hour for 30 min a 1 μm impactor was switched in line in order to provide an indication of the difference between submicron and total aerosol scattering.

2.5. Hygroscopicity Tandem Differential Mobility Analyzer (HTDMA, University of Manchester): $g(RH)$ at RH = 90%

[14] The HTDMA measured the increase in particle diameter from 35 to 90% RH for a preselected monodisperse particle population at nominal diameters of D_p = 40, 60, 89, 137, 217 and 360 nm with a temporal resolution of one hour [*Cubison et al.*, 2005]. Calibration for the offset in DMA sizing and variability in RH was achieved following the method of *Weingartner et al.* [2002] and verification of quantitative growth factor measurement using ammonium sulfate solution, referenced to well-described modeling in the literature [e.g., *Topping et al.*, 2005]. In an attempt to limit kinetic effects, the HTDMA ran a residence chamber of roughly one minute between the DMAs. The data retrieval based on an optimal estimation method was performed by the method described by *Cubison et al.* [2005]; this retrieval method was also able to determine the resolution of the instrument to be approximately 0.2 in $g(RH)$ space.

2.6. Aerosol Mass Spectrometer: Composition (Vacuum Aerodynamic Diameter D_{va} > 40 nm)

[15] The Aerodyne Aerosol Mass Spectrometer (AMS) [*Jayne et al.*, 2000; *Jimenez et al.*, 2003] measured the size-resolved mass concentrations in the range 30 nm to 1 μm. The AMS uses an aerodynamic lens to focus the particles into a narrow beam, a roughened cartridge heater to vaporize them under high vacuum, and electron impact ionization plus a quadrupole mass spectrometer to analyze the vaporized molecules. Particle size is measured via particle time-of-flight. Below about 80 nm the transmission falls off sharply, and at ~600 nm the transmission also falls off, decreasing to around 50% at a micron particle diameter [e.g., *Jayne et al.*, 2000], which corresponds approximately to the PM_1 definition. These effects are accounted for in the data analysis process used to calculate the relative composition for the CCN model. The AMS is operated in two modes: (1) a continuous mass spectrum mode without size information and (2) a size distribution measurement mode for selected mass-to-charge ratio settings of the quadrupole. More detailed descriptions of the AMS instrument are available from *Jayne et al.* [2000], and *Jimenez et al.* [2003], and a detailed description of the analysis technique is given by *Allan et al.* [2003, 2004]. The results of the AMS analyses for this study are presented by J. D. Allan et al. (In situ measurements of particle composition at Chebogue Point during ICARTT, unpublished manuscript, 2007, hereinafter referred to as Allan et al., unpublished manuscript, 2007).

2.7. Multiangle Absorption Photometer

[16] Light absorption measurements from a Multiangle Absorption Photometer (MAAP [*Petzold and Schönlinner*, 2004]) were converted to equivalent black carbon (EBC) concentrations using a mass absorption coefficient of 6.6 $m^2\ g^{-1}$. This factor was empirically calculated by the Thermo Electron company, which manufactures the MAAP instrument.

3. Model Calculations

[17] The input data to the model consists of 30-min average measurements. The following input data are used: (1) aerosol number concentration $N_{a,i}$ [cm^{-3}] in 55 size classes i (3 nm < D_p < 810 nm); (2) CCN concentrations at the (instrument) recorded supersaturations (S_1–S_5); (3) $f(RH)$ for three wavelengths, calculated at 85% RH and referenced to 40% RH; or (4) $g(RH)$ at six individual sizes (D_p = 40, 60, 89, 137, 217, 360 nm) at 90% RH. The approach to predicting CCN at the prescribed supersaturations is based on model calculations of particle uptake of water vapor for measured particle size distributions. The composition of the particles is constrained using $f(RH)$ (section 3.2) and, in a second set of calculations, using $g(RH)$ (section 3.3). Additional calculations have been performed using water vapor uptake calculations based on more detailed composition information from the AMS (section 3.5).

3.1. Hygroscopic Growth

[18] We introduce the simplified model of the equilibrium size of a wet particle of radius r, comprising soluble and insoluble fractions. The equilibrium saturation S_{eq}(= RH/100%) is described by the Köhler equation

$$S_{eq} = \exp\left[\frac{2M_w\sigma_s}{RT\rho_w r} - \frac{\nu\Phi M_w m_s/M_s}{\frac{4}{3}\pi\rho_{particle}r^3 - (m_s + m_{insol})}\right], \quad (1)$$

where M_w = molecular weight of water; σ_s = surface tension of the solution; R = ideal gas constant; T = temperature; ρ_w = density of water; $\nu\Phi \sim$ the van't Hoff factor, i.e., the product of the number of ions (ν) and the osmotic coefficient (Φ); M_s = molecular weight of the solute; $\rho_{particle}$ = density of the particle, m_s = soluble mass ($m_{total} - m_{insol}$), i.e.,

$$m_s = (1 - \epsilon)\ m_{total} \quad (2)$$

with m_{total} = total mass of aerosol particle and ε = insoluble mass fraction. The second term in equation (1) (the solute term) represents the ratio of moles of solute (= $f(\nu\Phi, M_s)$) to moles of water at a given relative humidity.

[19] Measurements of the aerosol particle composition at Chebogue Point during the measurement period show that

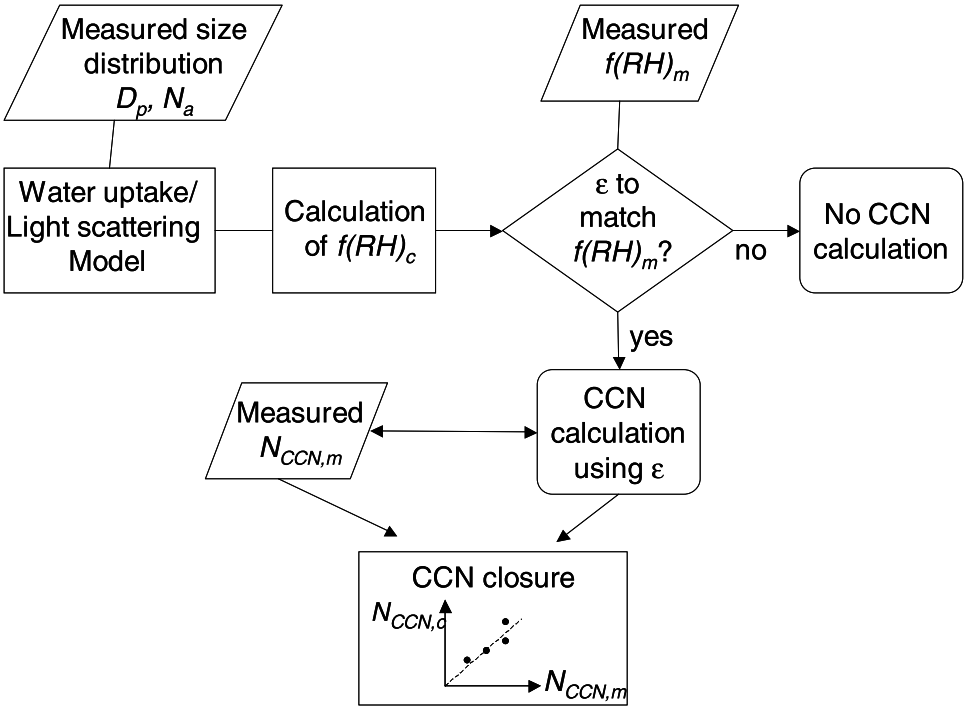

Figure 1. Schematic representation of model procedure. (The application of $g(RH)$ as a composition constraint was performed in the same way.)

ammonium and sulfate were the predominant inorganic components. The nitrate fraction was always small (<5%). The mole ratio of ammonium to sulfate during five selected periods during which we did a more detailed analysis of the importance of composition (see section 3.5) was always 2 or greater. On the basis of this analysis, we use ammonium sulfate $(NH_4)_2SO_4$ as a proxy for the soluble fraction of the aerosol. Its molecular weight is $M_s = 132$ g mol^{-1}, it is fully soluble, and its van't Hoff factor $\nu\Phi$ is calculated on the basis of a parameterization of the measurements by *Kunkel* [1969]. Note that all assumptions of the physicochemical properties also hold for periods during which the aerosol might not have been fully neutralized and ammonium bisulfate NH_4HSO_4 was the dominant inorganic solute (Allan et al., unpublished manuscript, 2007) because its hygroscopicity ($\propto \nu\Phi/M_s$) differs by <5% from that of ammonium sulfate. The model approach takes into account the hygroscopicity of particles in a simplified way by modeling the mole ratio of water/solute. It does not require detailed information on different solutes that are likely to exist in the aerosol (inorganics, organics). Similar ideas have been successfully applied by *Rissler et al.* [2004]. In section 3.5, we refine this model to account for more complex composition, e.g., soluble organics.

3.2. Optical Growth Factor *f*(*RH*) as a Composition Constraint

[20] The nephelometer measures the scattering of the aerosol population as an integrated value for the particle size range. In order to calculate the light scattering σ_{sp} of the discretized aerosol population we use Mie theory [e.g., *Bohren and Huffmann*, 1983].

$$\sigma_{sp} = \pi \sum_i r_i^2 Q_{scat}(m, r_i, \lambda) N_{a,i}, \tag{3}$$

where $N_{a,i}$ is the number concentration of particles with radius r_i (at a given RH) in size class i and the scattering efficiency Q_{scat} is a complex function of the particle size, refractive index m, and wavelength λ

$$Q_{scat} = f(m, r_i, \lambda). \tag{4}$$

For this application we used an average refractive index m for the total aerosol distribution of $m = 1.45 + 0.005$i, values derived from a comparison of the light scattering measured by a nephelometer ($\lambda = 450$ nm) for the analyzed data set to light scattering calculations (Mie theory) based on the measured aerosol size distribution measurements in this study. Calculations are performed at a reference RH = 40% ("dry") and at RH = 85% ("wet") to yield the enhancement in the total scattering σ_{sp} [m^2 m^{-3}] of the aerosol population. The optical growth factor $f(RH)$ is calculated for each of the individual measured size distributions, with

$$f(RH) = \frac{\sigma_{sp}(RH = 85\%)}{\sigma_{sp}(RH = 40\%)}. \tag{5}$$

[21] In a first approach, we apply the assumption as described in 3.1, namely that the aerosol is only composed of a soluble (with ammonium sulfate as proxy compound) fraction and an insoluble fraction ε. In order to constrain the mass fraction at each 30 min time step, the insoluble mass fraction ε is varied over the range $0\% < \varepsilon < 99\%$ (in 1% steps) until the model aerosol exhibits the same $f(RH)$ as the measured data (Figure 1). This approach is similar to those that have been suggested by *Rissler et al.* [2004] and *Petters and Kreidenweis* [2006] who suggested that hygroscopicity, and, thus, growth factors can be simply represented by the

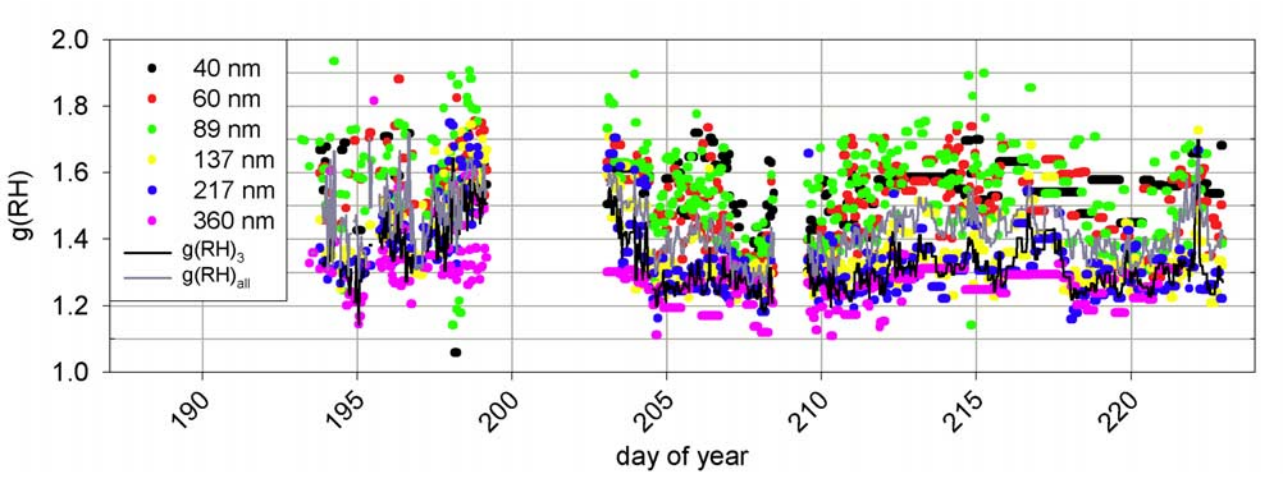

Figure 2. Measured growth factors for six particle sizes (40–360 nm) as a function of time. $g(RH)_3$ = average $g(RH)$ for largest three particle sizes, and $g(RH)_{all}$ = average $g(RH)$ for all sizes.

solute/water mole ratio without detailed knowledge of specific solute properties.

[22] As described previously, a RH of 40% was used as reference for the dry state of the particles. However, it is likely that the particles contain small amounts of water at RH = 40%. In order to correct the measurements for the remaining water mass one would have to make assumptions about the composition of the particle, which is exactly the property we seek to constrain through use of $f(RH)$. The effect of this small amount of water is that predicted insoluble fractions should be slightly smaller, with commensurate effects on activated number concentration. This effect is likely to be small relative to the uncertainties in many of the other properties.

3.3. Diameter Growth Factor $g(RH)$ as a Composition Constraint

[23] While $f(RH)$ represents an integrated value for the size distribution, the diameter growth factor $g(RH)$ is derived for individual particle sizes

$$g(RH) = \frac{r(i)_{wet}(RH = 90\%)}{r(i)_{dry}}. \tag{6}$$

During the experiment, growth factors were measured for six particle diameters (D_p = 40, 60, 89, 137, 217, 360 nm). The measured values as a function of particle size and time are shown in Figure 2. The fact that smaller particles exhibit higher $g(RH)$ than larger ones is inconsistent with a constant composition throughout the size range. It suggests rather that particles >100 nm contain less hygroscopic material.

[24] In our first set of modeling calculations we compare the applicability of $f(RH)$ and $g(RH)$ as a constraint on aerosol composition. Since the particle sizes that contribute most to scattering have sizes $D_p > 100$ nm we average only the $g(RH)$ values of the largest three sizes ($g(RH)_3$) and apply the same procedure to determine the composition (ε) as done for $f(RH)$. In additional calculations we investigate the extent to which CCN predictions change if an average of all $g(RH)$ values is applied ($g(RH)_{all}$).

3.4. Calculation of CCN Number

[25] The $(NH_4)_2SO_4/\varepsilon$ composition determined from this iterative process, using $f(RH)$ and $g(RH)$ as composition constraints, is then used to calculate the CCN number concentration at the five supersaturations (S_1–S_5) in the CCN instrument. It can be shown (equations (7)–(11)) that particles which have a dry radius greater than or equal to $r_{d,c}$ (the critical dry radius) are activated at a supersaturation S_{eq} (equation (1)) [*Pruppacher and Klett*, 1997]:

$$r_{d,c} = \left(\frac{r_{w,c}^3(A - S_{eq}r_{w,c})}{A + (B - S_{eq})r_{w,c}}\right)^{1/3} \tag{7}$$

with

$$A = \frac{2M_w\sigma_s}{RT\rho_w} \qquad B = \frac{\nu\Phi(1-\epsilon)M_w\rho_s}{M_s\rho_w} \tag{8}$$

with ρ_s = density of the solute. The activation radius $r_{w,c}$, i.e., the wet particle size at which the particles are activated, is calculated as

$$r_{w,c} = -\frac{D}{2} + \left(\frac{D^2}{4} - E\right)^{1/2} \tag{9}$$

with

$$D = \frac{2B^2A - 6BAS_{eq}}{3BS_{eq}^2 - 3B^2S_{eq}} \tag{10}$$

and

$$E = \frac{3BA^2}{3BS_{eq}^2 - 3B^2S_{eq}}. \tag{11}$$

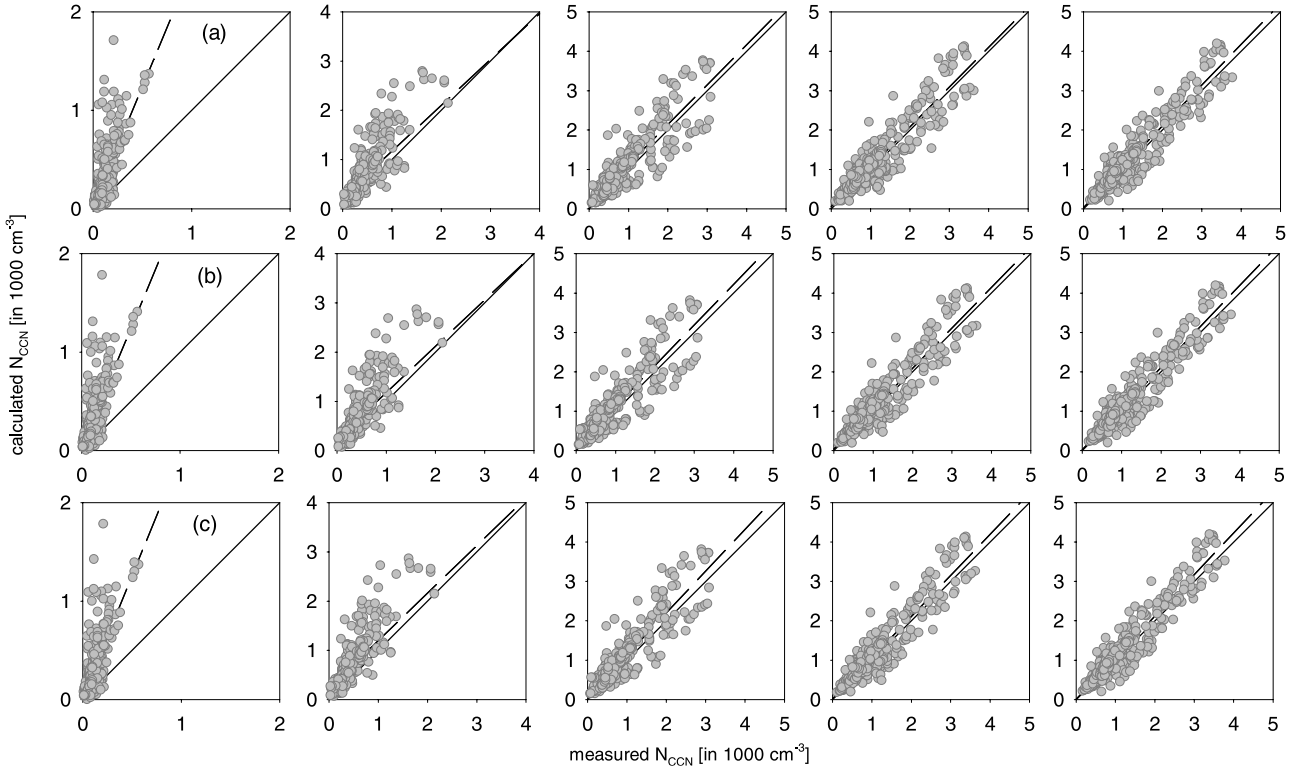

Figure 3. Calculated versus measured CCN number concentrations at five different supersaturations ($S_1 \sim 0.07\%$, $S_2 \sim 0.17\%$, $S_3 \sim 0.27\%$, $S_4 \sim 0.4\%$, and $S_5 \sim 0.5\%$) based on composition ($(NH_4)_2SO_4 + \varepsilon$) in order to match $f(RH)$ at RH = 85%. (a) λ = 700 nm ("red"), (b) λ = 550 nm ("green"), and (c) λ = 450 nm ("blue"). Dashed line is regression line.

3.5. Refinement of Aerosol Composition: Organic Fraction

[26] In a second application of the model, we have refined the previous approaches by considering more complex aerosol compositions and included information on organic, inorganic and EBC mass fractions derived from AMS and MAAP measurements for five selected periods. The inorganic fraction is assumed to be $(NH_4)_2SO_4$ and the organic fraction is assumed to have an average molecular weight M_s = 200 g mol^{-1} and van't Hoff factor $\nu\Phi = 1$. For the model calculations, an average density for all particles has been derived using the method of comparing electrical mobility and aerodynamic diameters described by *DeCarlo et al.* [2004].

[27] We apply this simple set of properties to the organic fraction and do not account for any deviations from ideal behavior (i.e., we assume $\Phi = 1$) as we lack information on that from the measurements. For the same reason, we also assume that the organic fraction forms an ideal solution; that is, we do not apply complex thermodynamic models [e.g., *Clegg et al.*, 2001; *Topping et al.*, 2005] in order to account for interactions between inorganic and organic components. Rather, we treat the water uptake on the aerosol by each component (organic/inorganic) separately, according to the ZSR approach [*Zdanovskii*, 1948; *Stokes and Robinson*, 1966]. It should be noted that the real composition of the organic fraction is likely much more complex than represented by only one compound (as defined by M, σ and $\nu\Phi$). We discuss the implications for particle growth under subsaturated and supersaturated conditions (i.e., growth factors and CCN activation, respectively) in section 5.3.

4. Results

4.1. *f(RH)*

[28] Figure 3 shows the measured versus predicted CCN number concentrations based on the measured size distribution and derived composition (as represented by ε) that produced a match between measured and calculated $f(RH)$ at the given wavelength. Table 1a summarizes the parameters of the regression lines for all plots in Figures 3a–3c. We only compare those data for which simultaneous measurements of N_a, $f(RH)$ at three wavelengths, and $g(RH)$ were available (400 samples). In less than ten cases the model was unable to match the measured growth factor ("No CCN calculation," in Figure 1). In these cases the growth factors exceeded the value that was predicted for pure ammonium sulfate ($\varepsilon = 0$).

[29] The difference between predicted and measured CCN is largest at S_1 but becomes progressively smaller at $S \geq S_2$ until the best fit regression fit approaches the 1:1 line. The consistent bias at S_1 can either be explained by inappropriate assumptions in the applied model that yields a CCN number that is too high or, alternatively, by uncertainties in the CCN instrument, which lead to small CCN numbers: The measured small CCN number concentration might suggest that the particles contain a significant fraction of insoluble material, which we calculated to be $\varepsilon \sim 0.88$.

Table 1a. Regression Line Parameters (Intercept a, Slope b) and Correlation Coefficients r^2 for Calculated Versus Measured CCN Number Concentrations Using Different Input Parameters in Order to Constrain the Aerosol Composition[a]

	S_1			S_2			S_3			S_4			S_5		
	a	b	r^2	a	b	r^2	a	b	r^2	a	b	r^2	a	b	r^2
$f(RH)_{blue}$	36	2.4	0.53	230	0.97	0.50	80	1.06	0.83	19	1.04	0.88	7	1.05	0.91
$f(RH)_{green}$	38	2.4	0.53	234	0.94	0.49	100	1.03	0.80	37	1.02	0.83	20	1.04	0.90
$f(RH)_{red}$	38	2.4	0.53	237	0.93	0.48	110	1.01	0.79	48	1.01	0.86	29	1.03	0.89
$g(RH)_3 \geq 137$ nm	46	2.7	0.53	215	1.16	0.57	66	1.22	0.91	38	1.12	0.90	18	1.13	0.94
$g(RH)_{all}$, 40–360 nm	52	3.3	0.55	263	1.26	0.57	106	1.27	0.91	80	1.14	0.90	52	1.14	0.93
Constant ε	68	2.3	0.42	262	0.95	0.51	96	1.10	0.88	64	1.05	0.86	60	1.06	0.88
Nominal S values	106	1.8	0.38	305	1.08	0.47	112	1.13	0.84	62	1.07	0.90	42	1.08	0.91

[a]All regressions are performed for the 400 data points for which a complete data set (S, $g(RH)$, $f(RH)$, and N_a) is available.

However, the AMS composition data do not support such high insoluble fraction as in all cases the inorganic fraction (which is composed mainly of ammonium, sulfate and nitrate) was always greater than 20%. In addition, the average growth factor of an aerosol population composed of ammonium sulfate and 88% insoluble material would be $g(RH) \sim 1.16$, which is significantly smaller than any of the time-dependent measured growth factors (Figure 2).

[30] It is possible in principle that a small fraction of the organic mass sometimes goes undetected by the AMS. However, the organic mass detected with the AMS compares well with the organic carbon measured with thermal-optical instruments and with the total volume or mass measured with instruments such as SMPS and TEOM (Tapered Element Oscillating Microbalance). If 5–10% of the organic mass was not detected by the AMS, this would likely be missed by such intercomparisons because of inherent scatter, or calibration uncertainties of all instruments, but such small deviations would not translate into uncertainties in the assumed inorganic/organic fractions that could explain the large bias at S_1.

[31] In order to explain the bias by instrumental uncertainties in the CCN counter a value of $S_1 \sim 0.03\%$ has to be assumed, a value deemed unrealistically low on the basis of the instrument model calculations. Examination of the manner in which the CCN counter was operated shows that the progressive overprediction of the CCN number concentration with decreasing S is a result of the higher than desirable flow rates in the CCN instrument: At small S, the flow rate of 0.5 L min^{-1} is large enough that droplets do not reach the size threshold of 0.75 μm above which they are detected by the optical particle counter (OPC). In future applications operation at lower flow rates is recommended to allow particles to grow to detectable sizes [*Lance et al.*, 2006].

[32] The regression coefficients for all supersaturations and $f(RH)$ data increase with decreasing wavelength. This is explained by Figure 4 where we have plotted the average distribution of all 400 size distributions (dry and humidified), as well as the total scattering σ_{sp} as a function of particle size (equation (4)) for all three wavelengths, at RH = 40% and RH = 85%. It is clear that the shortest (blue) wavelength is more sensitive to small particles than the longer wavelengths. Comparing the size ranges that contribute to scattering and the critical diameters at S_1 and S_5 it becomes evident that for this size distribution, $f(RH)$ contains composition information down to particle diameters of about 100 nm assuming a homogenous, internally mixed aerosol population throughout the size range. (For size distributions exhibiting a significant increase in the number of particles with decreasing size, the information content will extend to sizes smaller than 100 nm.) However, the fraction of the light scattering contributed by particles of size near the critical diameters (D_{crit1}–D_{crit5}) is very small. Thus the good performance of the CCN closure in Figure 3, in which the activation of small particles is predicted on the basis of scattering of larger particles, suggests relatively small differences in particle hygroscopicity over the range of sizes at this remote location where particles have had ample time to age. This closure exercise would likely be less successful, e.g., in an urban area where the sources and composition of the particles around D_{crit}, and the particles that dominate light scattering exhibit greater variability.

[33] In Figure 5, we show the corresponding insoluble fractions ε that are required in order to match the measured $f(RH)$. Using the three $f(RH)$ values, the predicted average is $\varepsilon \sim 0.63$. Approximately the same composition is predicted at all three wavelengths. An error in the nephelometer measurements and, thus, in $f(RH)$ of about 16% (section 2.4) translates into an error $\Delta\varepsilon \sim 0.3$ at $\varepsilon \sim 0.63$. The successful

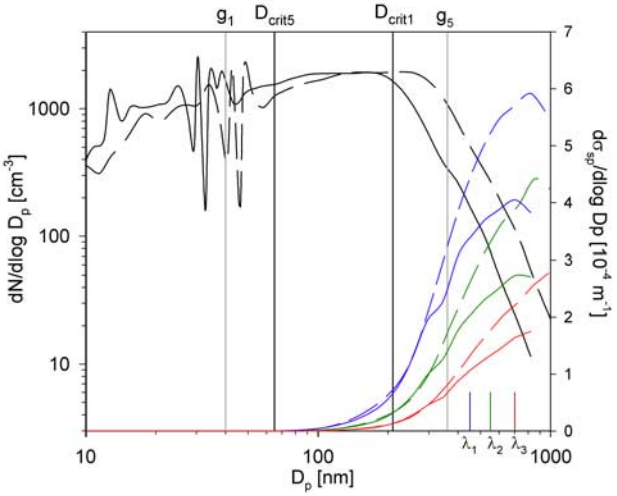

Figure 4. Average size distribution of 400 data points (black) and average scattering of aerosol population at λ = 450 nm (blue), λ = 550 nm (green); λ = 700 nm (red). g_1 and g_5 show the boundary sizes at which $g(RH)$ has been measured, and D_{crit1} and D_{crit5} are the average critical diameters for S_1 and S_5, respectively. Solid lines and dashed lines are for the dry and humidified distributions, respectively.

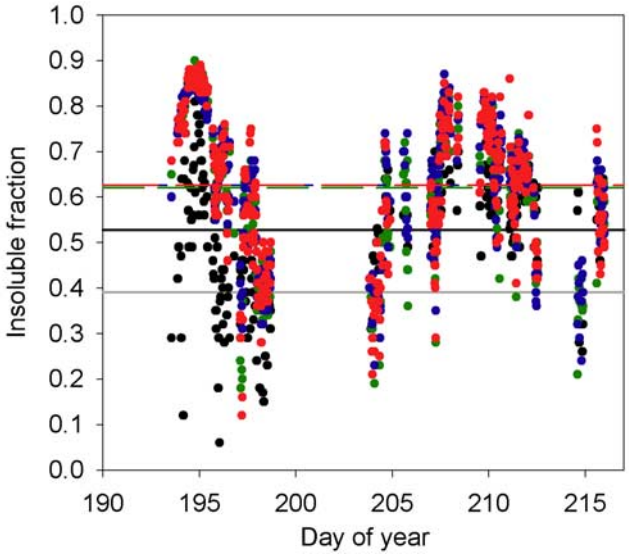

Figure 5. Predicted insoluble fraction, ε, based on $f(RH)$ at three wavelengths and on $g(RH)_3$. Predicted ε for $f(RH)$ are color coded by wavelength, black symbols indicate predicted ε for $g(RH)_3$, regression lines use the same color coding, and grey line indicates average ε based on $g(RH)_{all}$.

prediction of CCN based on this composition which includes particle diameters <100 nm (e.g., at S_5) suggests that the assumption of an internal mixture composition that is invariant with size is appropriate and any differences in hygroscopicity throughout the size range are small. Thus, for these conditions we show that composition information from any range of the size distribution can be used as a proxy for the whole size range. In the case of varying composition throughout the particle sizes, the application of $f(RH)$ in order to determine the composition for CCN relevant sizes is likely to be less successful.

4.2. *g(RH)*

[34] The growth factors $g(RH)$ were determined for six different sizes (40–360 nm). For some periods there is no clear difference between the measured growth factors in this size range (Figure 2); however, in general, the largest particles exhibit smaller $g(RH)$ values than particles <100 nm. This behavior cannot be explained by an internally mixed aerosol population as, all else being equal, smaller particles should have smaller $g(RH)$ because of the Kelvin (curvature) effect (first term on the right hand side of equation (1)). In a first approach we compare the data derived on the basis of both approaches of growth factor measurements ($f(RH)$ and $g(RH)$) and we use $g(RH)_3$ (i.e., $D_p > 100$ nm) since scattering is also dominated by particle sizes above this threshold. In addition, we also summarize regression parameters in Table 1a and Figure 6 that were derived on the basis of an average of all size growth factors $g(RH)_{all}$.

[35] The results in Figure 6 have been obtained using the same procedure as described in section 4.1 and Figure 1, except that now the water vapor uptake characteristics of the aerosol model are constrained by $g(RH)$. The composition (i.e., ε) is varied until the model matches the measured value $g(RH)_3$. This calculation is consistent with that of *Rissler et al.* [2004]. We see that the model using $g(RH)_3$ leads to an overestimate of the CCN number concentration that is small at high S but increases with decreasing S, and has less scatter than the comparison based on $f(RH)$ (Figure 3). The high bias in predicted CCN at S_1 is again primarily attributed to the large flow rate in the CCN counter and the inability of the OPC to detect the growing droplets. (Explanations based on composition variability with size, and/or mixing state cannot be ruled out but are deemed less likely.) At S_1, there is some small improvement in the slope of the regression (Table 1a) when an attempt is made to account for variability of composition with size (compare $g(RH)_3$ and $g(RH)_{all}$), but there remains a very strong overestimate in predicted CCN concentration. For this simple aerosol model, the composition measurements do not support the very high insoluble fraction ($\varepsilon = 0.88$) that would be required to match the small CCN number at low S. The general bias toward larger values of predicted CCN has been observed in previous closure studies for similar conditions, e.g., by *Broekhuizen et al.* [2006] who attributed the bias to poor size resolution.

[36] In Figure 5, the predicted insoluble fractions ε based on $g(RH)$ are compared to those obtained using $f(RH)$. It is evident that there is a systematic difference, with smaller insoluble fractions derived from $g(RH)_3$ (average ± standard deviation $\varepsilon \sim 0.53 \pm 0.14$, compared to $\varepsilon = 0.63 \pm 0.16$

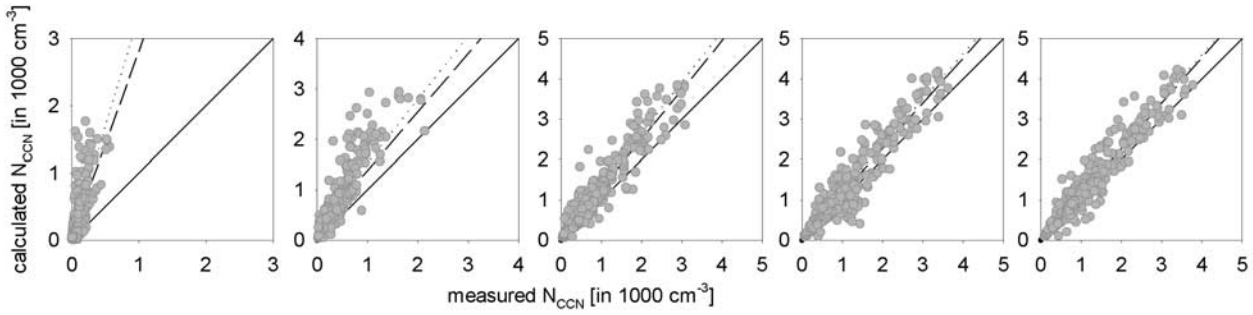

Figure 6. Calculated versus measured CCN number concentrations at five different supersaturations ($S_1 \sim 0.07\%$, $S_2 \sim 0.17\%$, $S_3 \sim 0.27\%$, $S_4 \sim 0.4\%$, and $S_5 \sim 0.5\%$) based on composition ($(NH_4)_2SO_4 + \varepsilon$) in order to match $g(RH)_3$ at RH = 90%. Dashed line indicates regression line; dotted line indicates regression line based on composition in order to match $g(RH)_{all}$.

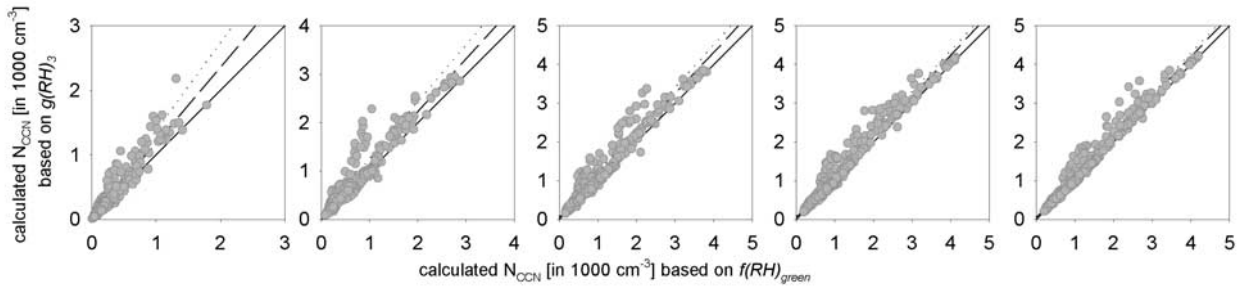

Figure 7. Calculated CCN number concentration based on composition ($(NH_4)_2SO_4 + \varepsilon$) in order to match $g(RH)_3$ at RH = 90% versus CCN number in order to match $f(RH)$ at RH = 85% (λ = 550 nm ("green")). Dashed line indicates regression line; dotted line indicates regression line based on composition in order to match $g(RH)_{all}$.

based on $f(RH)$). If the growth factors of the more hygroscopic particles are also included ($g(RH)_{all}$), $\varepsilon = 0.39 \pm 0.16$ is predicted.

4.3. Comparison of $f(RH)$ and $g(RH)$ Results

4.3.1. Agreement in Predicted CCN

[37] Both Figures 3 and 6 (and Table 1a) show a correlation $r^2 > 0.8$ between the predicted and measured CCN number concentrations for both $f(RH)$ and $g(RH)$ at $S \geq S_3$, with results improving with increasing S. In order to check if this is based on common agreement for the same data points, Figure 7 compares the calculated CCN numbers on the basis of $f(RH)_{green}$ and $g(RH)_3$. The agreement is worst at S_1 since use of $g(RH)_3$ leads to a greater overestimate of the CCN number than the data based on $f(RH)_{\text{green}}$ (see slope of regression lines in Table 1a). In Figure 5 we showed that the insoluble fraction ε derived from modeling $f(RH)$ was about 0.63 whereas the corresponding value based on $g(RH)_3$ is lower ($\varepsilon \sim 0.53$). However, at the higher supersaturations S_2–S_5 predictions based on $g(RH)$ and $f(RH)_{green}$ lead to CCN numbers that exhibit a small difference between the two predicted CCN number concentrations, which is reflected by the slope of the regression line of 1.15 to 0.98 at low and high S, respectively (Table 1b and Figure 7). At S_2–S_4, there are apparently two separate groups of data: Most of the points are close to the 1:1 line while a small fraction of the points shows a distinctly greater slope. The measurements for these few points were contiguous in time during a period with high organic fraction (see section 4.4.1, period 1). However, even a closer analysis of all available measurements for period 1 does not lead to any comprehensive explanation for the differences between the CCN calculated from $g(RH)$ and $f(RH)$ compared to the other data points.

4.3.2. Assumption of Constant ε

[38] In order to explore the extent to which the knowledge of the effective insoluble fraction is important for CCN prediction, we assumed a constant ε (37% $(NH_4)_2SO_4$/63% insoluble) for all data based on the $f(RH)$ composition modeling. Note that this ε could not have been known a priori. The results using $\varepsilon = 0.63$ are shown in Figure 8. In addition, we compare the parameters of the regression lines for these plots in Table 1a for the same data points as compared in Figures 3 and 6. At all supersaturations the slopes of the regression lines are comparable to those derived using variable ε. The variation of ε in the range we predict on the basis of $f(RH)$ and $g(RH)$ measurements leads to the same predicted CCN number concentration at higher S. This suggests that small differences in hygroscopicity (as implied by changing ε in equations (1)–(3), as a possible proxy for other aerosol composition properties in equation (1)) from the average for the period play a rather weak role for the activation of the aerosol sampled at Chebogue Point.

4.4. Increasing the Complexity of Aerosol Composition

4.4.1. Inorganic, Organic, Insoluble, and Equivalent Black Carbon Fraction

[39] Table 2 contains information about five different selected periods that have been chosen in order to analyze more closely the effects of aerosol composition on the calculated CCN. The periods have been selected on the basis of differences in composition, mass loading, and aerosol history. However, they can be classified into two broad groups: Periods 1, 2, and 5 exhibit high organic

Table 1b. Regression Line Parameters (Intercept a, Slope b) and Correlation Coefficients (r^2) for Calculated CCN Numbers Using $f(RH)_{\text{green}}$ Figure 3b and $g(RH)_3$ (Figure 6) as Composition Constraint (Figure 7)

	Predicted CCN Number Using $g(RH)_3$ Versus $f(RH)_{green}$
S_1	
a	49
b	1.15
r^2	0.90
S_2	
a	88
b	1.12
r^2	0.93
S_3	
a	97
b	0.99
r^2	0.96
S_4	
a	109
b	0.96
r^2	0.96
S_5	
a	58
b	0.98
r^2	0.98

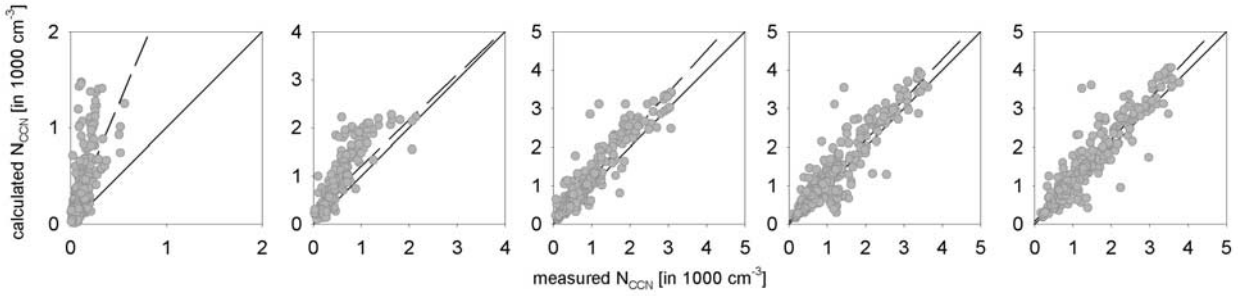

Figure 8. Calculated versus measured CCN number concentrations at five different supersaturations ($S_1 \sim 0.07\%$, $S_2 \sim 0.17\%$, $S_3 \sim 0.27\%$, $S_4 \sim 0.4\%$, and $S_5 \sim 0.5\%$), assuming a fixed composition of 37% $(NH_4)_2SO_4$/63% insoluble. Dashed line indicates regression line.

fractions, while during periods 3 and 4 the inorganic fraction dominates. For each of these periods we have defined mass fractions for inorganics, organics and EBC on the basis of the AMS and MAAP measurements. Particle composition is assumed to be constant with size and all particles are assumed to contain an internal mixture of the species present in the same mass proportions as in the average composition. Clearly this is still a simplified model since $g(RH)$ measurements indicate a change in composition with size (Figure 2).

[40] We assumed the properties for $(NH_4)_2SO_4$ for the inorganic fraction, since ammonium and sulfate are the predominant inorganic solutes (and NH_4HSO_4 has very similar hygroscopic properties), even though the aerosols had a more complex inorganic composition. Most of the organics at Chebogue Point can be classified as oxygenated organic aerosols (OOA) (Allan et al., unpublished manuscript, 2007). Recent results of field experiments in Tokyo indicate that about 90% of OOA detected with an AMS are water-soluble, as measured with the PILS-OC (Particle-in-liquid-sampler, organic carbon) technique [*Kondo et al.*, 2007].

[41] In order to check our previous predictions of the effective insoluble fraction ε we show in Figure 9 the measured organic fractions and equivalent black carbon fractions and the insoluble fraction as predicted from the calculations described in section 4.1, based on $f(RH)_{green}$ as a constraint (the error bars represent the standard deviation based on all predicted ε in the respective period). Assuming that all organics are effectively insoluble and the insoluble fraction of the aerosol is composed only of EBC and organics, the difference between the measured and the predicted insoluble fractions is in all cases less than 10%. The inference that almost all of the organic mass can be modeled as effectively insoluble seemingly contradicts the previous classification of OOA as water-soluble. A possible reason for this discrepancy might be differences between the OOA solubility in Tokyo and Chebogue Point. A more likely explanation is that particles at RH = 85% do not contain much water (water/solute mass ratio $\sim$ 1) and, thus, organics of limited solubility might not be fully dissolved. At high ionic concentrations in the aqueous phase organics might form a separate phase because of the "salting out" effect which leads to an even smaller apparent solubility. In the PILS-OC instrument the organic mass is diluted to typical concentrations of $1–2 \cdot 10^{-4}$ g L^{-1} water (100–200 ppb kg^{-1} (R. Weber, personal communication, 2006)). Our results suggest that most of the water-soluble organic carbon determined in analyses such as the PILS-OC might not influence the particle growth by water uptake at subsaturated conditions.

[42] In Figure 10 the comparison is shown of the predicted CCN number concentration based on $f(RH)_{green}$ using the $(NH_4)_2SO_4/\varepsilon$ model and the more complex directly measured composition described in Table 2. Both are plotted as a function of the measured CCN concentrations. Unlike the composition variation performed in sections 4.1 and 4.2 where ε was varied over the total aerosol mass, the variation of the insoluble fraction is now only done over the organic fraction (ε'). In most cases, this approach is not able to match the measured $f(RH)_{green}$ values since it requires even more insoluble mass than is represented by $\varepsilon' = 1$ (organic + EBC fraction = insoluble). Therefore we show the predicted CCN for the boundary value of $\varepsilon' = 1$ (i.e., organics modeled as completely insoluble) for all periods. It is noted that in some cases when the AMS and MAAP data are included in the calculations, there is a marginal improvement in the predicted number of CCN (e.g., period 5).

Table 2. Composition ($(NH_4)_2SO_4$/Organic/EBC) and Aerosol Distribution Details for Individual Periods (Average)

Period	Time, day of year	Mass Fractions: Inorganic $(NH_4)_2SO_4$	Mass Fractions: Organic	Mass Fractions: Equivalent Black Carbon (EBC)	$\varepsilon_{predicted}$ Based on $f(RH)_{green}$	Density, g cm^{-3}	Mass Loading, μg m^{-3}	Particle Number Concentration, cm^{-3}	Characteristics
1	195.01–195.43	0.229	0.705	0.066	0.83	1.31	8.0	3,961	high organics/EBC
2	196.08–196.50	0.397	0.571	0.032	0.66	1.33	2.9	771	clean, bimodal
3	197.46–197.73	0.660	0.328	0.012	0.32	1.49	17.7	4,177	high sulfate
4	204.19–204.46	0.693	0.279	0.028	0.38	1.38	4.8	1,621	fairly clean
5	209.76–209.97	0.17	0.805	0.025	0.79	1.18	9.4	10,941	high organics

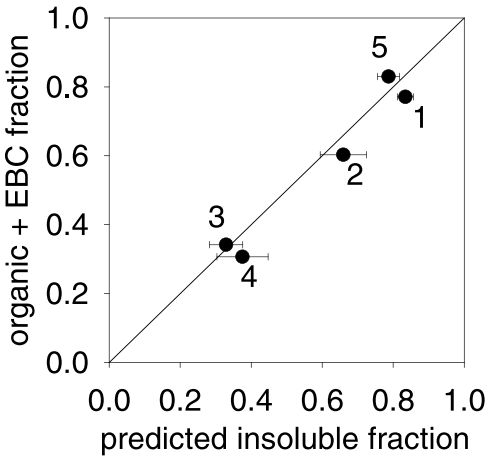

Figure 9. Comparison of insoluble fraction calculated on the basis of $f(RH)_{green}$ and measured mass fractions of EBC + organics (numbers indicate periods; Table 2). Error bars represent the standard deviation of all ε for the individual data points in the respective period.

However, in general the benefit of the additional complexity in the aerosol model is small.

[43] In previous CCN closure studies it has been assumed that all organics are insoluble, and that the remainder of the aerosol mass contains additional insoluble material. Even this assumption can lead to an overestimate of the CCN numbers by about 25% [*Broekhuizen et al.*, 2006]. In this latter study, it is suggested that the agreement in the CCN closure might be improved with more detailed information on (1) size-resolved composition and (2) the mixing state of the aerosol population, i.e., the existence of completely insoluble and soluble particles of the same size (external mixture).

[44] For our model calculations we have assumed an internal mixture for all particles. As $g(RH)$ measurements are performed for single particles at selected sizes an externally mixed aerosol population will result in a growth factor distribution. On the basis of the uncertainty of the instrument ($\Delta g(RH) = 0.2$) we cannot fully exclude the possibility of externally mixed aerosols. However, the hygroscopicity of particles having different compositions was very similar, i.e., within the range of the instrument's uncertainty. The uncertainty in $g(RH)$ of about 0.2 translates into $\Delta\varepsilon \sim 0.3$. As shown in section 4.3.2, the assumption of a constant value for ε did not change the predicted CCN significantly for the retrieved range of ε between ~0.3 and 0.9 (Figure 5). Nevertheless, inaccuracies in $g(RH)$ measurements need to be considered in retrievals of this kind.

4.4.2. Additional Information on Composition

4.4.2.1. Size-Resolved Composition

[45] In addition to the size-averaged composition given in Table 2, we have used size-resolved information on composition. Information was available for particles greater than

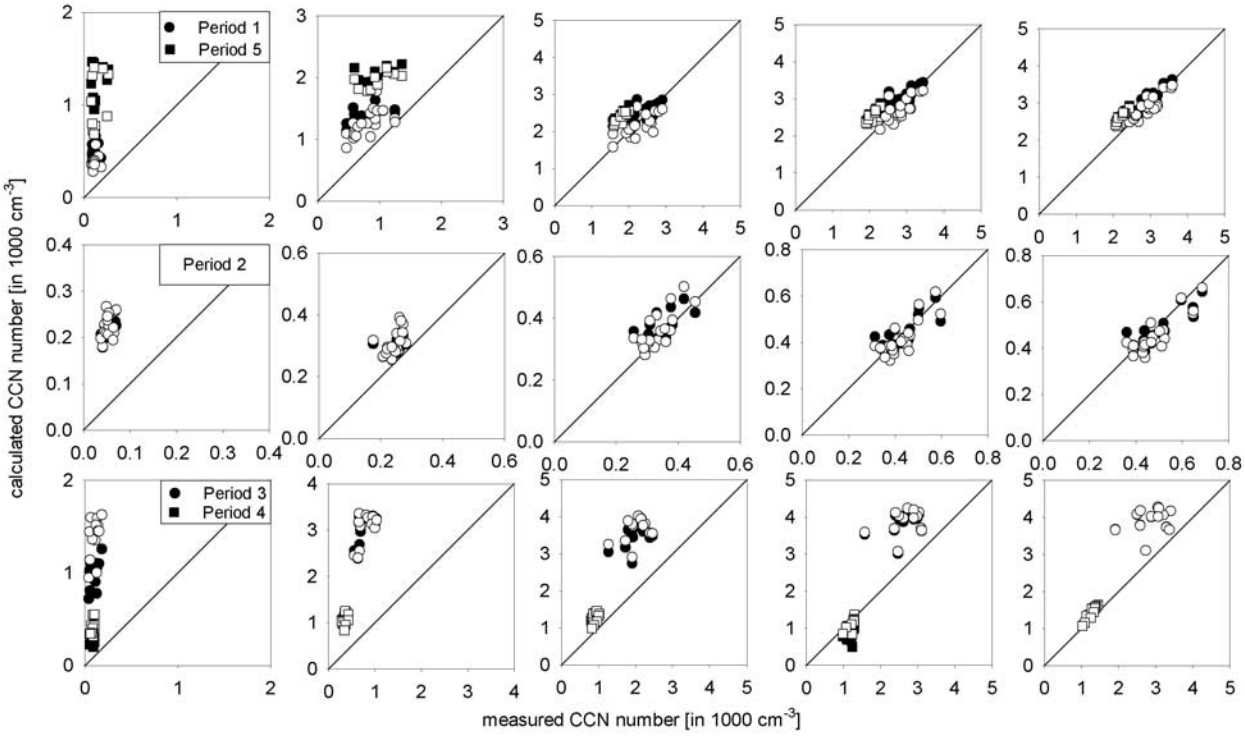

Figure 10. Calculated versus measured CCN number concentrations at five different supersaturations ($S_1 \sim 0.07\%$, $S_2 \sim 0.17\%$, $S_3 \sim 0.27\%$, $S_4 \sim 0.4\%$, and $S_5 \sim 0.5\%$) based on full composition information. Open symbols indicate ($(NH_4)_2SO_4 + \varepsilon$); solid symbols indicate composition as specified in Table 2, $\varepsilon' = 1$ (see text for details).

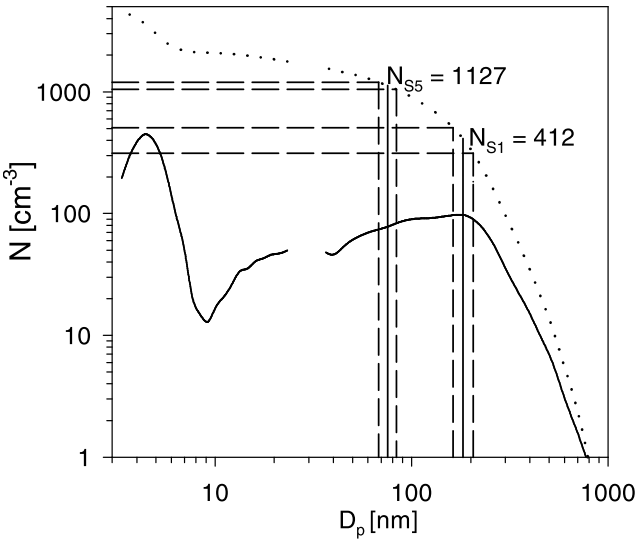

Figure 11. Schematic of size distribution and critical diameters (vertical lines) and the assessment of relative uncertainty in predicted CCN number concentration. Solid line indicates average size distribution, and dotted line indicates cumulative size distribution.

D_{va} = 100 nm (vacuum aerodynamic diameter [*DeCarlo et al.*, 2004]) for three different size ranges (100–250 nm, 250–700 nm, >700 nm). The EBC fraction is assumed constant for all size classes since it was determined from the absorption properties of the total aerosol population and we have no means of apportioning it by size. The insoluble fraction of these calculations was assumed to be $\varepsilon' = 1$, as in section 4.4.1. Because of the lack of further information we had to make assumptions about the composition of particles smaller than D_{va} = 100 nm and varied their composition between 99% insoluble and completely soluble ammonium sulfate. Even this refinement of the composition did not lead to any improvement in the agreement between measured and predicted CCN numbers compared to Figure 10. Results are therefore not shown.

4.4.2.2. Refractive Index of Organic Fraction

[46] The refractive index of the internally mixed inorganic/organic aerosol, as used in the model calculations in the previous sections, is based on the consistency between measured optical properties and calculations based on aerosol size distributions over the entire measurement campaign. The refractive index of organic aerosol constituents is poorly constrained. Since no further specification of the organic fraction for our specific data set is available, we have explored the possible effects of refractive index of the organics by considering the range of values found in literature studies for organics in different locations. We have found that even the variation from m = 1.53 [*Malm et al.*, 2005], to $m = 1.43 - 0.0035$ i [*Gelencsér*, 2004] does not lead to any significant change in predicted CCN number concentration. (In the interests of brevity, results are not shown.)

4.4.2.3. Density of Organic Fraction

[47] The densities given in Table 2 represent average densities for the total aerosol population during the individual periods, derived from the closure of the AMS and SMPS size distributions [*DeCarlo et al.*, 2004]. The average density of OOA which were predominant at Chebogue Point has been determined as ρ_{org} = 1.4 g cm^{-3} [*Cross et al.*, 2007]. If we disregard the average densities used in the previous section, but use the explicit densities for all mass fractions as individual input parameters we did not observe any significant improvement in the prediction of CCN.

5. Discussion

5.1. Critical Radius, *S*, and Size Distribution

[48] Figures 3, 6, and 7 show higher correlation coefficients r^2 (Table 1) between measured and predicted CCN number at higher supersaturation for both $f(RH)$- and $g(RH)$-derived values. In this section we discuss the reasons for higher uncertainty in CCN prediction at low S. The relationship between the properties of an activated particle and the critical supersaturation is given by equations (7)–(11). By assuming a uniform composition throughout the size distribution we can determine the minimum dry size ($r_{d,c}$ in equation (7)) of the activated particles for any given size distribution and supersaturation. In Figure 11, we show the average of all 400 size distributions, the cumulative number concentration and the two average critical diameters (D_{crit1} and D_{crit5}) at S_1 and S_5, respectively. We assume an uncertainty in the activated sizes of one size bin (dashed, vertical lines). Since the diameter bins in the size distribution are logarithmically distributed, this assumption leads to the same relative uncertainty in size. This uncertainty translates into a difference in activated particle numbers ΔN_S as shown by the differences between the horizontal lines at each of the critical diameters. We calculate the relative error δ

$$\delta = \frac{\Delta N_S}{N_S^{tot}} \tag{12}$$

in the total number of activated particles N_S^{tot} and find that $\delta_1 = 194/412 = 0.47$; and $\delta_5 = 152/1127 = 0.13$). At low S (i.e., large sizes), δ is about 3.5 times greater than at high S. This is because in the latter case a major fraction of the aerosol population is activated, and any uncertainties in activation of additional particles represent a smaller fraction of the total activated number that leads to a smaller relative change. (The magnitude of these differences will vary with size distribution shape but the general picture is clear.) This estimate of uncertainty only explains the scattering of the points around the regression line (precision). Any systematic bias as explained previously, e.g., due to instrumental uncertainties, leads to error in the accuracy of the CCN predictions (intercept and slopes of regression lines) that are independent of the relative uncertainty (Table 1).

5.2. Calculation of Supersaturation

[49] As stated in section 2, the nominal values of S_1 have been corrected by means of the model by *Lance et al.* [2006] in order to account for small temporal deviations in the temperature profile in the CCN counter. In order to explore the extent to which this correction of S at each 30 min time step improves agreement between predicted and measured CCN, we repeated the calculations from Figure 3b ($f(RH)_{green}$) but used the nominal S values (S_1 = 0.09%, S_2 = 0.21%, S_3 = 0.32%, S_4 = 0.43% S_5 = 0.55%) as

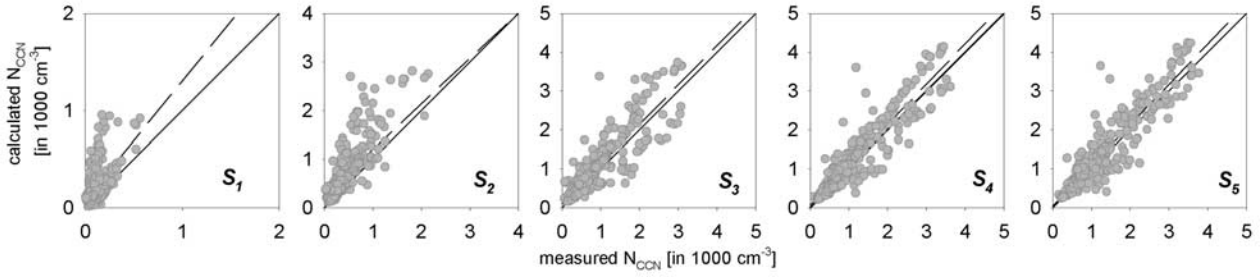

Figure 12. Calculated versus measured CCN numbers at five different supersaturations (nominal values of the CCN counter: S_1 = 0.09%, S_2 = 0.22%, S_3 = 0.32%, S_4 = 0.45%, and S_5 = 0.55%) based on composition ($(NH_4)_2SO_4 + \varepsilon$) in order to match $f(RH)$ at RH = 85% (λ = 550 nm ("green")). Dashed line indicates regression line.

specified by the instrument for the duration of the experiment. The results are shown in Figure 12 and the corresponding regression parameters listed in Table 1a. For $S \geq S_2$, the assumption of the constant nominal supersaturation values over the whole time period does not bias the results significantly, for the reasons discussed in section 5.1.

5.3. Complexity of Organic Fraction

[50] As pointed out previously, no information on the organic properties relevant for hygroscopicity could be derived on the basis of the AMS data. This omission leads to some uncertainties in the description of aerosol composition and hygroscopicity. The set of properties we have chosen for the organic fraction reflects a single compound with a relatively small molecular weight (M_s = 200 g mol^{-1}), that does not affect surface tension, and that forms an ideal mixture with other (inorganic) water-soluble compounds. This representation of the organic fraction is greatly simplified as it has been shown that the organic fraction of atmospheric aerosol can be composed of hundreds of different compounds with a broad range of physicochemical properties. A large fraction of this organic fraction can be composed of high molecular weight components that reduce the surface tension of aqueous particles and might not be fully miscible with water [e.g., *Decesari et al.*, 2000].

[51] As shown in the modeling study by *Ervens et al.* [2005], at subsaturated conditions, the particle growth is dominated by the solute term ($\propto r^{-3}$; second term in equation (1)) as the Kelvin term ($\propto r^{-1}$; first term in equation (1)) is small at small particle radii. Thus hygroscopic growth is mainly determined by molecular weight M_s and the van't Hoff factor $\nu\Phi$. If the van't Hoff factor also increases with increasing molecular weight (e.g., the polarity and water-miscibility of the compound decrease) both parameters will have an opposite effect. In general, organic compounds can reduce the surface tension of aqueous particles which in turn decreases the critical diameter of activation (equations (7)–(11)). High molecular weight compounds have the most distinct effect on surface tension reduction. However, the surface tension of aqueous solutions is concentration-dependent, and with increasing particle size the solutions are more dilute and the surface tension effect is reduced. We cannot quantify the extent to which organic properties counter each other. However, we point out that these properties should be considered together, and that their combined effects might weaken the influence of organic properties on hygroscopic growth and particle activation.

6. Summary and Conclusions

6.1. What Is the Relative Usefulness of $f(RH)$ Versus $g(RH)$?

[52] We have used measured size distributions and optical ($f(RH)$) or diameter ($g(RH)$) hygroscopic growth factor measurements at RH = 85% and RH = 90%, respectively, to predict CCN number concentrations. The data were obtained over a period of four weeks during July/August 2004, at Chebogue Point, Nova Scotia, Canada, as part of the ICARTT study. To our knowledge this is the first study in which (1) $f(RH)$ has been used to extrapolate growth information of aerosols at subsaturated conditions to their CCN activity and (2) the resulting CCN number predictions have been compared to those based on $g(RH)$ measurements.

[53] The current results suggest that for this data set either of these growth factors can be used to give reliable predictions of CCN number at supersaturations $S > \sim 0.3\%$. We hypothesize, on the basis of the current analysis, that similar success could have been achieved at lower S, had lower CCN flow rates been applied during the experiment, but this cannot be verified a posteriori. In addition, we cannot completely rule out the possibility that assumptions about composition at the large particle sizes and/or uncertainty in $g(RH)$ measurements play a role in the poor retrievals at low S.

[54] It should also be pointed out here that $f(RH)$ retrievals may be less effective if the composition of the aerosol population versus size is not as homogeneous as in the present study. In the presence of several modes that are composed of different species, as more typically observed in an urban area, it is unclear how useful the observed growth characteristics based on $f(RH)$ will be for inferring CCN properties.

6.2. What Information Is Most Crucial for CCN Prediction?

[55] The data set acquired at Chebogue Point during the ICARTT field study included detailed information on aerosol properties, namely time-resolved measurements of size

Table 3. Relative Importance of Several Parameters Regarding CCN Predictions for the Data Set at Chebogue Point During the ICARTT Study (Internally Mixed Aerosol Population With Homogeneous Composition for Size Range)

Parameter	Relative Importance
Size distribution	high
Supersaturation	high
Composition	low
Size-resolved composition	low
Soluble fraction (number of soluble moles) as function of particle size	moderate
(Organic) solute properties	low

distribution, number concentration, and size-resolved composition. In addition, three different $f(RH)$, $g(RH)$ at six different particle sizes, and a sophisticated approach to determine the exact supersaturation at which the CCN number concentration was measured, were available. Such a detailed data set is rarely available from field studies. On the basis of our numerous sensitivity tests, we provide guidance in Table 3 as to what information is most crucial for future successful CCN closure experiments for similar conditions. We caution that these conclusions pertain specifically to the data from Chebogue Point and may not always be appropriate. As shown in Table 3, the most important information for CCN closure is the measured aerosol size distribution and the supersaturation. A simple representation of aerosol composition based on an internally mixed soluble/insoluble mixture, constrained by either $g(RH)$ or $f(RH)$, appears to be quite adequate, especially at high supersaturations. This supports the notion that the water uptake by oxygenated organic aerosol in concentrated solutions is negligible and the organic fraction can be modeled as water-insoluble (equations (1) and (2)). Temporal variation in composition, and even the variability in composition with size (e.g., as reflected in $g(RH)$ measurements), does not appear to be of great importance during the period of study at Chebogue Point even in periods when organic species clearly dominate the aerosol mass. Attempting to refine the composition using measured equivalent black carbon and organic fractions does not contribute significantly to an improvement in the agreement between predicted and measured CCN number concentrations. If hygroscopic growth information is unavailable, predictions of CCN may still be feasible provided some a priori composition information is available (e.g., insoluble fraction and appropriate parameterization of the solute properties). This conclusion is in general agreement with the parameterization by *Fitzgerald* [1975] that shows a correlation between the insoluble fraction and CCN number for a constant composition of an aerosol population that is internally mixed.

[56] Note that the requirement of accurate knowledge of S in the CCN instrument is important for successful closure, but not for independent CCN predictions. Measured size distribution and hygroscopic information should suffice for routine CCN predictions. Similar conclusions have been drawn by *Rissler et al.* [2004] and *Dusek et al.* [2006] on the basis of analysis of Brazilian biomass burning aerosol and aerosol in central Germany, respectively. However, in these latter studies the lowest supersaturation at which CCN analyses were performed were 0.33% and 0.4%, respectively, which corresponds approximately to S_3 and S_4 in our study. In all these studies, it has been consistently found that with decreasing supersaturation the CCN measurements are more sensitive to instrumental conditions and counting statistics.

[57] CCN closure studies describe particle activation under equilibrium conditions. They represent an important step toward our understanding of the role of aerosol particles in cloud formation processes. In order to give a more realistic picture of cloud formation, dynamic processes also have to be considered as has been done in a recent study by *Ervens et al.* [2005], who examined the effect of composition on cloud droplet number concentration. There it was shown that only significant changes ($\sim$factor of 5) in the solute term will change the cloud drop number concentration appreciably ($\sim$15%), with the importance increasing with decreasing updraft velocities and increasing aerosol number concentration. Sensitivity to composition in CCN measurements does not necessarily translate into sensitivity in drop number concentration as in a rising air parcel both the time for particle growth and the amount of available water vapor are limited and, thus, effects of competition for water vapor might influence the growth rates of particles.

[58] Further aerosol measurements and model studies are required to extend our understanding of the relationship between aerosol and cloud properties. The extent remains to be seen to which the conclusions we have drawn from our current study hold true for other locations and aerosol conditions where there is more complexity in aerosol composition and mixing state and to which aerosol activation behavior can be parameterized in order to describe cloud processes properly.

[59] **Acknowledgments.** We thank James Allan (University of Manchester), J. Alex Huffman (University of Colorado), Doug Worsnop, Eben Cross, Megan Northway, and Manjula Canagaratna (Aerodyne Research Institute) for AMS operation and data processing and Patrick Sheridan and Anne Jefferson for building, setting up, and operating the NOAA/ESRL instrumentation in the field. The DMPS and HTDMA instruments were deployed by the University of Manchester, and M. Cubison was supported through NERC studentship 06424 as a University of Manchester student during the period of the field campaign and initial analysis. B.E., E.A., G.F., and J.O. acknowledge funding from the NOAA Climate Goal. J.L.J., M.C., and P.F.D. thank NSF (CAREER grant ATM-0449815) and NOAA (grant NA05OAR4310025) for funding. P.F.D. is grateful for an EPA STAR Fellowship (FP-91650801).

References

Allan, J. D., J. L. Jimenez, P. I. Williams, M. R. Alfarra, K. N. Bower, J. T. Jayne, H. Coe, and D. R. Worsnop (2003), Quantitative sampling using an Aerodyne aerosol mass spectrometer: 1. Techniques of data interpretation and error analysis, *J. Geophys. Res.*, *108*(D3), 4090, doi:10.1029/2002JD002358.

Allan, J. D., et al. (2004), Technical note: Extraction of chemically resolved mass spectra from Aerodyne aerosol mass spectrometer data, *J. Aerosol Sci.*, *35*, 909–922.

Bohren, C. F., and D. R. Huffmann (1983), *Absorption and Scattering by Small Particles*, John Wiley, Hoboken, N. J.

Brechtel, F. J., and S. M. Kreidenweis (2000), Predicting particle critical supersaturation from hygroscopic growth measurements in the humidified TDMA. Part I: Theory and sensitivity studies, *J. Atmos. Sci.*, *57*, 1854–1871.

Broekhuizen, K., R. Y.-W. Chang, W. R. Leaitch, S.-M. Li, and J. P. D. Abbatt (2006), Closure between measured and modeled cloud condensation nuclei (CCN) using size-resolved aerosol compositions in downtown Toronto, *Atmos. Chem. Phys.*, *6*, 2513–2524.

Clarke, A. D., et al. (2002), INDOEX aerosol: A comparison and summary of chemical, microphysical, an optical properties observed from land, ship and aircraft, *J. Geophys. Res.*, *107*(D19), 8033, doi:10.1029/2001JD000572.

Clegg, S. L., J. H. Seinfeld, and P. Brimblecombe (2001), Thermodynamic modelling of aqueous aerosols containing electrolytes and dissolved organic compounds, *J. Aerosol Sci.*, *32*(6), 713–738.

Covert, D. S., R. J. Charlson, and N. C. Ahlquist (1972), A study of the relationship of chemical composition and humidity to light scattering by aerosols, *J. Appl. Meteorol.*, *11*, 968–976.

Covert, D. S., J. L. Gras, and A. Wiedensohler (1998), Comparison of directly measured CCN with CCN modeled from the number-size distribution in the marine boundary layer during ACE 1 at Cape Grim, Tasmania, *J. Geophys. Res.*, *103*(D13), 16,597–16,608.

Cross, E. S., J. G. Slowik, P. Davidovits, J. D. Allan, D. R. Worsnop, J. T. Jayne, D. K. Lewis, M. Canagaratna, and T. B. Onasch (2007), Laboratory and ambient particle density determinations using light scattering in conjunction with aerosol mass spectrometry, *Aerosol Sci. Technol.*, in press.

Cubison, M., H. Coe, and M. Gysel (2005), A modified hygroscopic tandem DMA and a data retrieval method based on optimal estimation, *J. Aerosol Sci.*, *36*(7), 846–865.

DeCarlo, P., J. G. Slowik, D. Worsnop, P. Davidovits, and J. Jimenez (2004), Particle morphology and density characterization by combined mobility and aerodynamic diameter measurements. Part 1: Theory, *Aerosol Sci. Technol.*, *38*, 1185–1205, doi:10.1080/027868290903907.

Decesari, S., M. C. Facchini, S. Fuzzi, and E. Tagliavani (2000), Characterization of water-soluble organic compounds in atmospheric aerosol: A new approach, *J. Geophys. Res.*, *105*(D1), 1481–1489.

Dusek, U., D. S. Covert, A. Wiedensohler, C. Neusüß, D. Weise, and W. Cantrell (2003), Cloud condensation nuclei spectra derived from size distributions and hygroscopic properties of the aerosol in coastal southwest Portugal during ACE-2, *Tellus, Ser. B*, *55*, 35–53.

Dusek, U., et al. (2006), Size matters more than chemistry in controlling which aerosol particles can nucleate cloud droplets, *Science*, *312*, 1375–1378.

Ervens, B., G. Feingold, and S. M. Kreidenweis (2005), The influence of water-soluble organic carbon on cloud drop number concentration, *J. Geophys. Res.*, *110*, D18211, doi:10.1029/2004JD005634.

Fitzgerald, J. W. (1975), Approximation formulas for the equilibrium size of an aerosol particle as a function of its dry size and composition and the ambient relative humidity, *J. Appl. Meteorol.*, *14*, 1044–1049.

Gelencsér, A. (2004), *Carbonaceous Aerosol*, Springer, New York.

Hämeri, K., C. D. O'Dowd, and C. Hoell (2002), Evaluating measurements of new particle concentrations, source rates, and spatial scales during coastal nucleation events using condensation particle counters, *J. Geophys. Res.*, *107*(D19), 8101, doi:10.1029/2001JD000411.

Jayne, J. T., D. C. Leard, X. Zhang, P. Davidovits, K. A. Smith, C. E. Kolb, and D. R. Worsnop (2000), Development of an aerosol mass spectrometer for size and composition analysis of submicron particles, *Aerosol Sci. Technol.*, *33*, 49–70.

Jimenez, J. L., et al. (2003), Ambient aerosol sampling with an aerosol mass spectrometer, *J. Geophys. Res.*, *108*(D7), 8425, doi:10.1029/2001JD001213.

Kasten, F. (1969), Visibility forecast in the phase of pre-condensation, *Tellus*, *21*, 631–635.

Kondo, Y., Y. Miyazaki, N. Takegawa, T. Miyakawa, R. J. Weber, J. L. Jimenez, Q. Zhang, and D. R. Worsnop (2007), Oxygenated and water-soluble organic aerosols in Tokyo, *J. Geophys. Res.*, *112*, D01203, doi:10.1029/2006JD007056.

Kotchenruther, R. A., P. V. Hobbs, and D. A. Hegg (1999), Humidification factors for atmospheric aerosols off the mid-Atlantic coast of the United States, *J. Geophys. Res.*, *104*, 2239–2251.

Kunkel, B. A. (1969), Comments on "A generalized equation for the solution effect in droplet growth," *J. Atmos. Sci.*, *26*, 1344–1346.

Lance, S., J. Medina, J. N. Smith, and A. Nenes (2006), Mapping the operation of the DMT continuous flow CCN counter, *Aerosol Sci. Technol.*, *40*(4), 242–254.

Liu, P. S. K., W. R. Leatich, C. M. Banic, S.-M. Li, D. Ngo, and W. J. Megaw (1996), Aerosol observations at Chebogue Point during the 1993 North Atlantic Regional Experiment: Relationships among cloud condensation nuclei, size distribution, and chemistry, *J. Geophys. Res.*, *101*(D22), 28,971–28,990.

Malm, W. C., D. E. Day, C. Carrico, S. M. Kreidenweis, J. L. Collett Jr., G. McMeeking, T. Lee, J. Carrillo, and B. Schichtel (2005), Intercomparison and closure calculations using measurements of aerosol species and optical properties during the Yosemite Aerosol Characterization study, *J. Geophys. Res.*, *110*, D14302, doi:10.1029/2004JD005494.

McInnes, L., M. Bergin, J. Ogren, and S. Schwartz (1998), Apportionment of light scattering and hygroscopic growth to aerosol composition, *Geophys. Res. Lett.*, *25*(4), 513–516.

Nenes, A., P. Y. Chuang, R. Flagan, and J. H. Seinfeld (2001), A theoretical analysis of cloud condensation nucleus (CCN) instruments, *J. Geophys. Res.*, *106*(D4), 3449–3474.

Petters, M. D., and S. M. Kreidenweis (2006), A single parameter representation of hygroscopic growth and cloud condensation nuclei activity, *Atmos. Chem. Phys. Disc.*, *6*, 8435–8456.

Petzold, A., and M. Schönlinner (2004), Multi-angle absorption photometry—A new method for the measurement of aerosol light absorption and atmospheric black carbon, *J. Aerosol Sci.*, *35*(4), 421–441.

Pruppacher, H. R., and J. D. Klett (1997), *Microphysics of Clouds and Precipitation*, Springer, New York.

Rader, D. J., and P. H. McMurry (1986), Application of the tandem differential mobility analyser for studies of droplet growth or evaporation, *J. Aerosol Sci.*, *17*, 771–787.

Rissler, J., E. Swietlicki, J. Zhou, G. Roberts, M. O. Andreae, L. V. Gatti, and P. Artaxo (2004), Physical properties of the sub-micrometer aerosol over the Amazon rain forest during the wet-to-dry season transition—Comparison of modeled and measured CCN concentrations, *Atmos. Chem. Phys.*, *4*, 2119–2143.

Roberts, G., and A. Nenes (2005), A continuous-flow streamwise thermal-gradient CCN chamber for atmospheric measurements, *Aerosol Sci. Technol.*, *39*(3), 206–221.

Snider, J. R., and J. Brenguier (2000), Cloud condensation nuclei and cloud droplet measurements during ACE-2, *Tellus, Ser. B*, *32*, 828–842.

Stokes, R. H., and R. A. Robinson (1966), Interactions in non-electrolyte solution I. Solute-solvent equilibria, *J. Phys. Chem.*, *70*, 2126–2130.

Topping, D. T., G. McFiggans, and H. Coe (2005), A curved multi-component aerosol hygroscopicity model framework: 1—Inorganics, *Atmos. Chem. Phys.*, *5*, 1223–1242.

Twomey, S. (1977), *Atmospheric Aerosols*, 302 pp., Elsevier, New York.

Weingartner, E., M. Gysel, and U. Baltensperger (2002), Hygroscopicity of aerosol particles at low temperatures. 1. New low-temperature H-TDMA instrument: setup and first applications, *Environ. Sci. Technol.*, *36*, 55–62.

Williams, P. I., M. W. Gallagher, T. W. Choularton, H. Coe, K. N. Bower, and G. McFiggans (2000), Aerosol development and interaction in an urban plume, *Aerosol Sci. Technol.*, *32*(2), 120–126.

Zdanovskii, A. B. (1948), New methods of calculating solubilities of electrolytes in multicomponent systems, *Zh. Fiz. Khim.*, *22*, 1475–1485.

E. Andrews, G. Feingold, and J. A. Ogren, Earth System Research Laboratory, NOAA, Boulder, CO 80305, USA.

M. Cubison, P. DeCarlo, and J. L. Jimenez, Cooperative Institute for Research in Environmental Sciences, University of Colorado, Boulder, CO 80309-0216, USA.

B. Ervens, Atmospheric Science Department, Colorado State University, Fort Collins, CO 80523, USA. (barbara.ervens@noaa.gov)

A. Nenes, School of Earth and Atmospheric Sciences, Georgia Institute of Technology, Atlanta, GA 30332, USA.